



# Rheology of semi-dilute suspensions with a viscoelastic matrix

Shaocong Dai<sup>1</sup> · Roger I. Tanner<sup>1</sup>

Received: 17 March 2020 / Revised: 12 May 2020 / Accepted: 19 May 2020 / Published online: 30 May 2020  
© Springer-Verlag GmbH Germany, part of Springer Nature 2020

## Abstract

This work explores the rheology of suspensions of spheres in a viscoelastic matrix. The volume fraction varies from zero to 0.2. Steady shearing, small strain sinusoidal shearing and uniaxial elongation are considered. We conclude that the matrix response in shear and elongation is fairly well described by a single-mode Oldroyd-B model, but the small-strain storage modulus ( $G'$ ) response is less well represented by such a model. The use of a two-mode Oldroyd-B model gives significant improvement. For the suspensions, the viscometric functions  $\eta$ ,  $N_1$  and  $N_2$  are given for volume fractions of 5, 10 and 20%, plus the oscillatory responses  $G'$ ,  $G''$  at 1% strain amplitude. The uniaxial elongation data show a very large increase in flow resistance relative to the matrix; for the same applied force, the rate of elongation decreases from about  $17.5 \text{ s}^{-1}$  for the matrix to about  $3 \text{ s}^{-1}$  for the suspensions. It appears that this large increase in resistance is due to areas of intense extension attached to two adjacent spheres, as has been demonstrated numerically. It is shown that a single-mode Oldroyd-B model cannot describe suspension behaviour. A two-mode Oldroyd-B model can capture the macroscopic behaviour of the suspensions but only if an initial Hencky strain of order 4 is present in the extending suspension filaments. A two-mode model of the matrix fluid also allows one to understand the suspension response from the microscopic view.

**Keywords** Suspensions · Viscoelasticity · Semi-dilute · Elongation · Shearing · Initial strain

## Introduction

The behaviour of suspensions with non-Newtonian matrix fluids has been discussed in several reviews (Metzner 1985; Shaqfeh 2019; Tanner 2019). It is clear that the local flow around the suspended spheres is quite complex and the characterization and modelling of the matrix rheology is very important. As a minimum, the behaviour in steady viscometric flows (the viscosity  $\eta$  and the two normal stress differences  $N_1$  and  $N_2$ ) should be measured, but only in rare cases (Dai et al. 2014; Tanner et al. 2015) are all three functions available. There are few measurements of extensional behaviour, in spite of their importance in suspension rheology (Hwang et al. 2004). Unsteady flow properties are also of interest and measurements of  $G'$ ,  $G''$  are relevant to modelling.

Here, we will first give experimental results for  $\eta$ ,  $N_1$ ,  $N_2$ ,  $G'$ ,  $G''$  and uniaxial extensional flow properties for the Boger

fluid used by Dai et al. (2014). The modelling of the fluid as an Oldroyd-B material will also be discussed. The behaviour of semi-dilute suspensions using this matrix fluid is then presented and discussed.

## Matrix fluid rheology

The viscoelastic matrix fluid used here and by Dai et al. (2014) was formed from corn syrup (79.42% by weight), glycerine (19.8%), water (0.75%) and a small amount (0.03%) of polyacrylic acid (PAA) with a molecular weight of  $5 \times 10^6 \text{ g/mol}$ . A similar matrix fluid was used by Zarraga et al. (2001). The matrix density was  $1352 \text{ kg/m}^3$ , and the viscosity at  $24 \text{ }^\circ\text{C}$  was about  $2.16 \text{ Pa s}$ .  $N_2$  was found to be too small to measure ( $< 0.1 \text{ Pa}$ ) and is assumed, from the results of Dai et al. (2014), to be zero. The matrix viscosity and first normal stress behaviour as functions of shear rate were measured using a Paar Physica MCR302 rheometer and are shown in Table 1 (top row). The viscosities were somewhat higher than those reported by Zarraga et al. (2001) possibly due to differences in the PAA molecular weights.

✉ Roger I. Tanner  
roger.tanner@sydney.edu.au

<sup>1</sup> School of Aerospace, Mechanical and Mechatronic Engineering,  
University of Sydney, Sydney, NSW 2006, Australia

**Table 1** Viscosity ( $\eta_o$ ) and normal stress coefficients for the matrix fluid (0%) and semi-dilute suspensions (5, 10 and 20% volume fractions)

$\varphi$ (%)	$\eta_o$ (Pa-s)	$N_1/\dot{\gamma}^2$ (Pa-s <sup>2</sup> )	$N_2/\dot{\gamma}^2$ (Pa-s <sup>2</sup> )
0	2.16	0.116	0
5	2.69	0.147	-0.0074
10	3.58	0.271	-0.0145
20	6.10	0.422	-0.0870

Modelling of the matrix as a second-order fluid was adopted by Dai et al. (2014); the second-order fluid had a negligible  $N_2$ . If  $N_1 = 0.116 \dot{\gamma}^2$  as in Table 1 and  $\eta_o$  is 2.16 Pa-s, then the relaxation time  $\lambda(= \frac{N_1}{2\eta_o \dot{\gamma}})$  is 0.027 s. However, it is equally possible and is preferable to regard the results of Table 1 via an Oldroyd-B model as did Vázquez-Quesada et al. (2019). They considered the matrix fluid to have a viscosity of 2.08 Pa-s of which the ‘polymer’ contribution was 0.666 Pa-s and a relaxation time of 0.084 s. Yang et al. (2016) described the same fluid as a Giesekus model with a relaxation time ( $\lambda$ ) of 0.09 s,  $\eta_o = 2.2$  Pa-s and a ‘polymer’ viscosity of 0.704 Pa-s; the Giesekus parameter  $\alpha$  was fitted to be 0.0034. This model was able to describe the droop away from the square law in  $N_1$  near a shear rate of  $100s^{-1}$ .

The modelling of the matrix fluid as an Oldroyd-B fluid in steady viscometric flow is seen to be generally satisfactory. The single relaxation time  $\lambda$  is assumed equal to 0.087 s, the mean of the values from the works of Vázquez-Quesada et al. (2019) and Yang et al. (2016). The single-mode Oldroyd-B stress tensor ( $\sigma$ ) for general flows can be written as follows:

$$\sigma = -p\mathbf{I} + 2\eta_s \mathbf{d} + \tau \tag{1}$$

Here, the pressure  $p$  in the assumed incompressible fluid is determined by the momentum balance. The Newtonian part of the matrix viscosity is  $\eta_s$  ( $= 1.469$  Pa.s in this case) and  $\mathbf{d}$  is the rate of deformation tensor. The extra stress  $\tau$  due to the polymeric component is described by an upper-convected Maxwell element:

$$\lambda \Delta \tau / \Delta t + \tau = 2\eta_p \mathbf{d} \tag{2}$$

In the present case  $\eta_p = 0.691$  Pa.s, so the total shear viscosity is 2.16 Pa.s;  $\eta_p/\eta_o = 0.32$ . The upper convected derivative term in Eq. 2 is as follows:

$$\Delta \tau / \Delta t = \{ \partial \tau / \partial t + \mathbf{v} \cdot \nabla \tau - \tau \mathbf{L}^T - \mathbf{L} \tau \} \tag{3}$$

where  $t$  is time,  $\mathbf{v}$  is the velocity vector and  $\nabla$  is the gradient operator.  $\mathbf{L}$  is the transpose of the velocity gradient ( $\nabla \mathbf{v}$ ) (Tanner 2000).

This model has the following properties:

\*Steady shearing—constant viscosity ( $\eta_o = \eta_s + \eta_p$ ), here equal to 2.16 Pa.s

\*First normal stress difference  $N_1$  equal to  $2\lambda \eta_p \dot{\gamma}^2$ ; or  $0.116 \dot{\gamma}^2$  in this case, where  $\dot{\gamma}$  is the shear rate

\*The second normal stress difference ( $N_2$ ) is zero.

\*In small—strain oscillatory flow ( $\gamma = \hat{\gamma} \sin \omega t$ ), one finds

$$G' = \lambda \eta_p \omega^2 / (1 + (\lambda \omega)^2) \tag{4}$$

$$G'' = \eta_s \omega + \eta_p \omega / (1 + (\lambda \omega)^2) \tag{5}$$

where  $\lambda = 0.087$  s and  $\omega$  is the frequency in rad/s.

For the papers cited here, there seems to be no record of the small strain behaviour. To rectify this for the sinusoidal small strain case (1% strain), the results for  $G'$  and  $G''$  are shown in Fig. 1.

Each experimental determination used three samples denoted by  $\blacklozenge$ ,  $\blacktriangle$  and  $\blacksquare$ . The Oldroyd-B model results (Eqs. 4 and 5) are shown by the + symbols.

The agreement between the experiments in Fig. 1 and Eqs. 4 and 5 is fair, and more modes would reduce the difference. Overall, the agreement with the model in simple and oscillatory shearing is considered reasonable. We now consider uniaxial elongational flow.

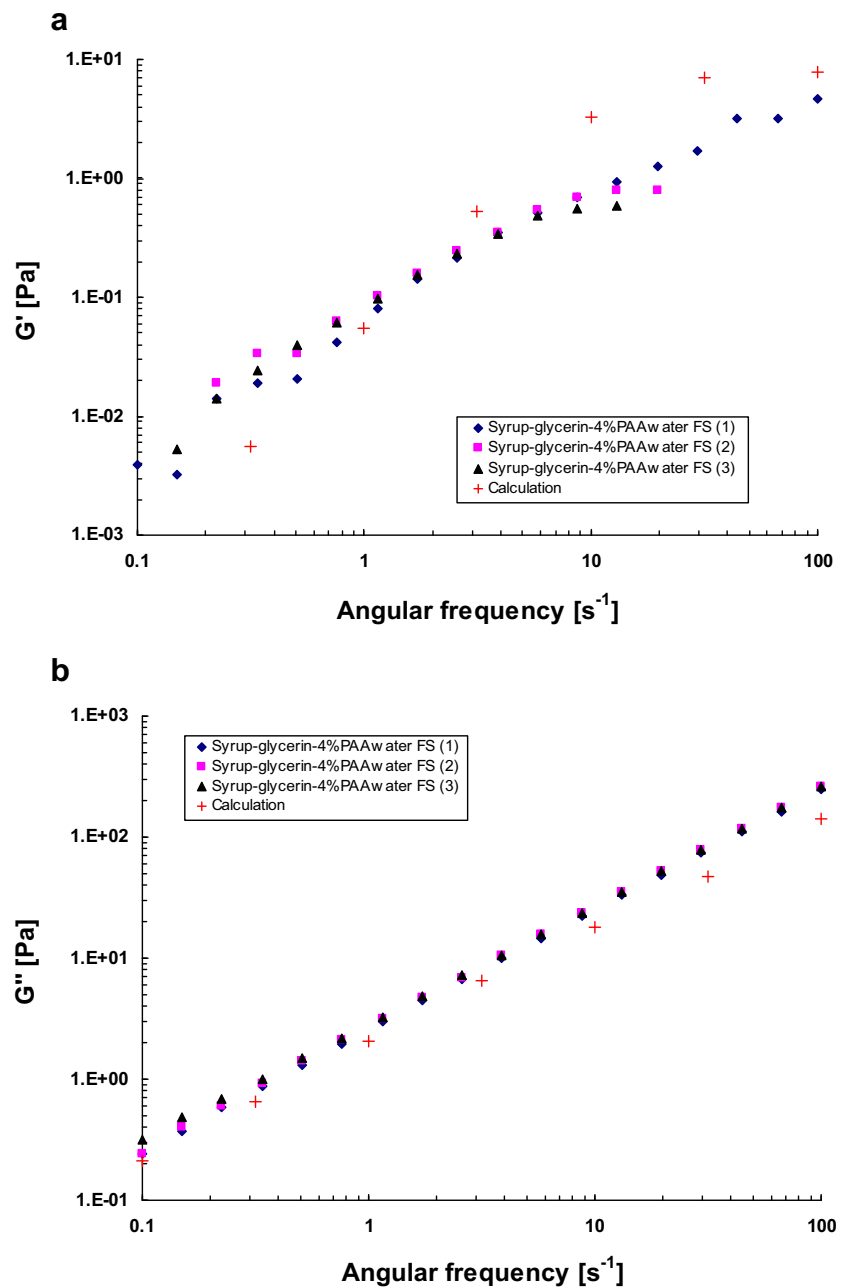
For the Oldroyd-B model in uniaxial elongation, there is no steady state at Weissenberg (Wi) numbers  $> 0.5$ . In the analysis, we will assume that the rate of strain ( $\dot{\epsilon}$ ) is constant; if this is not the case then the analysis of experimental results needs computation.

When the strain-rate is constant, the solution for the axial stress  $\sigma$  in the Oldroyd-B model can be re-arranged as a function of the Hencky strain ( $\epsilon = \dot{\epsilon} t$ ) and is, using the notation  $Wi = \lambda \dot{\epsilon}$ :

$$\sigma = 3\eta_s \dot{\epsilon} + 2\eta_p \dot{\epsilon} \{ 1 - \exp[-(2-1/Wi)\epsilon] \} / (1-2Wi) + \eta_p \dot{\epsilon} \{ 1 - \exp[-(1+1/Wi)\epsilon] \} / (1+Wi) \tag{6}$$

When  $\lambda = 0$  or the strain-rate is very small this reduces to  $\eta_o \dot{\epsilon}$ . It is assumed in the derivation of Eq. 6 that the stretch rate

**Fig. 1**  $G'$ ,  $G''$  for the matrix fluid at 1% strain amplitude. Three separate tests were made at each frequency and the (+) symbols are the result of the Oldroyd-B model where the polymer viscosity is 0.691 Pa.s, the viscous component is 1.469 Pa.s, and the relaxation time is 0.087 s



is suddenly applied at  $t = 0$ ; at that time the polymer does not contribute to the stress. The results of Eq. 6 will be compared with experiments.

Whilst the shearing tests are routine, the measurement of elongational flow is more difficult. We used the weight of the fluid with or without an embedded steel ball to apply the load and studied the development of the filament using a high-speed camera (Mahmud et al. 2018).

About 20 ml of fluid was put into the glass funnel and it flowed out through the attached capillary tube having 3.8 mm inner diameter (Fig. 2).

A high-speed FASTCAM PCI R2 (Photron) camera was used to film the motion of the fluid with a recording rate of 250 fps (frames per second), where the exposure time was 1 ms. In this experiment, following Mahmud et al. (2018), we measured the diameter and length of the extending filament and the volume of the drop from the images taken by the high-speed camera. At the central section, the flow was clearly elongational and the length of the filament was measured as a function of time, which enabled the value of the mean elongation rate ( $\dot{\epsilon}$ ) to be found. If the length of the filament at zero time is  $L_0$ , then, for a constant rate of strain the length  $L$  equals

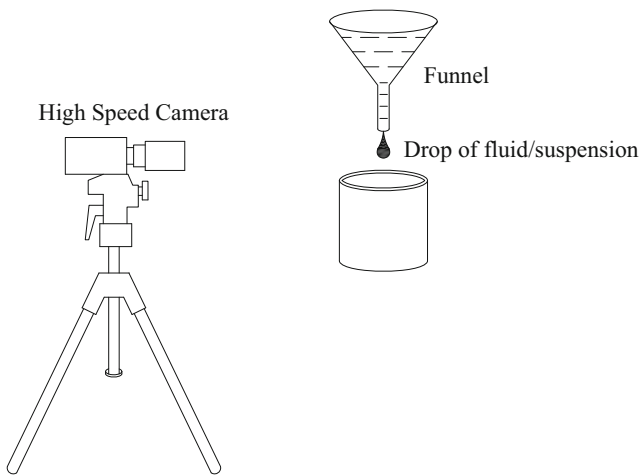
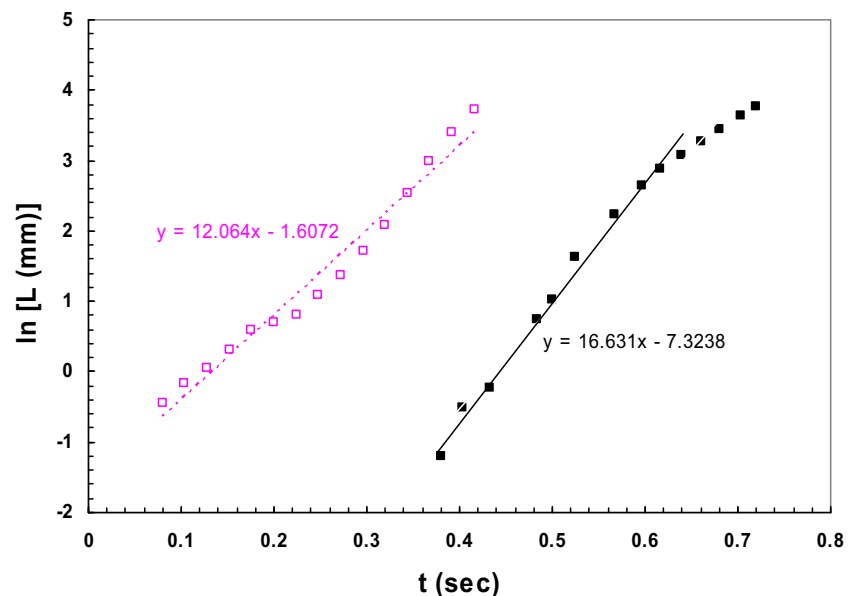


**Fig. 2** Sketch of falling-drop experiment. The drop of fluid contained in some cases a steel ball which increased the load on the filament and increased the uniformity of the filament

$L_0 \exp \dot{\epsilon} t$ . From Fig. 3, one sees that for the matrix fluid with an embedded ball, the exponential form assumed for the length  $L$  generally holds well, at least over an initial period, and so the rate of strain can be found from the slope of the lines in Fig. 3. The mean filament diameter  $d = d_0 \exp(-\dot{\epsilon} t/2)$  as is well-known. It was found that a much improved filament shape ensued if a small 3.17 mm diameter steel ball (mass 0.1303 g) was extruded with the fluid (Mahmud et al. 2018). This increased the load and the extension rate. It also allows more precise estimates of the filament length ( $L$ ) to be made, and only the results with embedded balls are analysed in detail here.

Because the filament thins rapidly in time, it is difficult to measure  $d$  accurately for longer times, and so the assumption is made that the volume of fluid in the filament is constant and

**Fig. 3** Length ( $L$ ) of filament as a function of time. The right-hand curve with the steel ball shows a constant rate of elongation of  $17.5 \text{ s}^{-1}$  in the initial stages. The left-hand curve has a complex rate of extension at an average rate of extension of about  $12 \text{ s}^{-1}$



equal to that near the beginning of the extension. Since the actual test time on the matrix filaments is much less than 1 s (Fig. 3), this assumption is considered fair; also one sees the volume of fluid at the fluid exit and around the ball is a very small fraction of the total filament volume. Knowing the filament length  $L$  as a function of time, the mean diameter  $d$  may then also be found as a function of time.

To find the load on the filament, the acceleration ( $\alpha$ ) of the steel ball (or the leading blob when there is no ball) is needed. For a constant  $\dot{\epsilon}$ , the acceleration of the ball is given by  $d^2L/dt^2$ , or

$$\alpha = \dot{\epsilon}^2 L \quad (7)$$

For the matrix fluid tests  $\alpha$  is a maximum of about  $1 \text{ m/s}^2$ ; if  $\dot{\epsilon}$  is not constant, then the acceleration must be found numerically. The stress at any strain can be found for the mid-point of the filament from the force  $F$  exerted on the filament by the ball (or blob) plus half of the mass of the filament:

$$F = (m + \pi \rho d^2 L/8) \{g - \alpha\} \quad (8)$$

where  $m$  is the mass of the embedded ball,  $\rho$  is the fluid density and  $g$  is the acceleration of gravity.

The apparent axial stress  $4F/\pi d^2$  is borne by the axial stress  $\sigma$  in the fluid plus a contribution of the surface tension (Mahmud et al. 2018) of  $2\sigma_s/d$ , where the surface tension coefficient  $\sigma_s$  was measured as 0.07 Pa-m. Subtracting  $2\sigma_s/d$  from the apparent axial stress gives the uniaxial stress  $\sigma$  in the fluid, which can be compared with the analytical solution (6).

From the photo images the position of the ball as a function of time could be found and the acceleration of the fluid blob/steel ball could be estimated from Eq. 7. The whole test

took about 0.3 s and generated about 100 photos. The acceleration ( $\alpha$ ) was found to be at most of order  $1 \text{ m/s}^2$  which is fairly small relative to the gravitational acceleration  $g$  ( $9.81 \text{ m/s}^2$ ). Hence, the load at the mid-length of the filament could be found as the (mass of ball + 0.5 of the mass of the filament) times ( $g - \alpha$ ). For the steel ball case, the total load was about 1 mN. In order to find the stresses, it is necessary to find the filament diameter at the mid-length. For small times this can be measured from the enlarged photographs, but eventually this becomes inaccurate. Hence, the diameter was found at later times by finding the volume of the fluid at small times and assuming that the product of the filament length and the square of the diameter remained constant. We considered the images at 0.02 s time intervals and calculated the length ( $L$ ) of the filament as a function of time (Fig. 3); from these data, the Hencky strain ( $\varepsilon = \ln(L/L_0)$ ) as a function of time could be found. We found by plotting  $L$  vs. time (Fig. 3) that for the case with the steel ball the rate of elongation ( $\dot{\varepsilon}$ ) was nearly constant at  $17.5 \text{ s}^{-1}$  over the initial time rate of elongation and then it reduced.

From Fig. 3, the behaviour of the filament without the steel ball results in an average rate of strain of about  $12 \text{ s}^{-1}$ , but in fact the rate of strain for times greater than about 0.22 s is nearly  $17.5 \text{ s}^{-1}$ ; in the centre and around  $t = 0.2 \text{ s}$ , there is a period of lower extension rate. In view of this complex result, it was decided that only the results with the embedded steel balls would be used.

The load on the fluid column in the experiments is due to the (reduced) weight of the ball and half of the column, but there is also a component due to surface tension, as mentioned above. From previous work (Mahmud et al. 2018), an extra force increases the apparent stress in the filament by  $\sigma_s/r$ , where  $\sigma_s$  is the surface tension coefficient (measured as 0.07 Pa.m) and  $r$  is the radius of the filament. Unlike this previous work which used silicone oil of larger viscosity, and where surface tension was smaller, in the present case the load borne by the fluid in the filament had to be reduced by the surface tension component in order to compare with the prediction from the Oldroyd-B model in Eq. 6, where no surface tension was considered.

The results for the axial stress  $\sigma$  are shown as a function of the Hencky strain  $\varepsilon$  in Fig. 4 (circles); here, the steel ball was used. Hence, it appears that the single-mode Oldroyd-B model represents the matrix rheology adequately. From Fig. 4, one sees that there are deviations in the experimental stresses of about  $\pm 20\%$ . We now consider suspension rheology.

## Suspension rheology

In order to minimize the effects of interparticle friction, which plays an important role when the volume fraction is greater

than about 0.25, the volume fractions considered here are restricted to 5, 10 and 20% (Tanner et al. 2015). The polystyrene (PS) spheres used were described by Dai et al. (2014) and were approximately  $40 \mu$  in diameter with a comparatively small average roughness of 0.15% of the sphere radius. The shear viscosity of the suspensions was constant up to Weissenberg numbers ( $Wi = \lambda \dot{\gamma}$ ) of about 0.9; thereafter, mild shear thickening occurred (Tanner 2019; Dai et al. 2014); the relaxation time of the matrix fluid is  $\lambda = 0.087 \text{ s}$ . The constant viscosities at lower  $Wi$  are reported in Table 1 along with the normal stress data.

The small shear strain data ( $G'$ ,  $G''$ ) are shown in Fig. 5a, b; a strain amplitude of 1% was imposed.

Using the same embedded ball technique described above, the uniaxial elongation behaviour was studied. The lengths of the filament ( $L$ ) as a function of time are shown in Fig. 6. Again, one sees exponential increases in length with time, so  $\dot{\varepsilon}$  is nearly constant and  $\dot{\varepsilon}t$  is the Hencky strain. Roughly, the load on the filament was always  $\sim 1.5 \text{ mN}$ , but the resulting rates of extension varied widely as the volume fraction was varied, see Table 2.

The presence of just a 5% volume fraction of spheres reduces the rate of extension dramatically, given the same load (Table 2). To provide a dimensionless plot of the behaviour, the results derived from Fig. 6 are shown in Fig. 7, where the dimensionless stress  $\sigma^*$  ( $= \sigma/3\eta_0 \dot{\varepsilon}$ ) is shown as a function of  $\varepsilon$  ( $= \ln(L/L_0)$ ). The value of  $L_0$  was chosen to be 3.2 mm (one embedded ball diameter) as seen in Fig. 6.

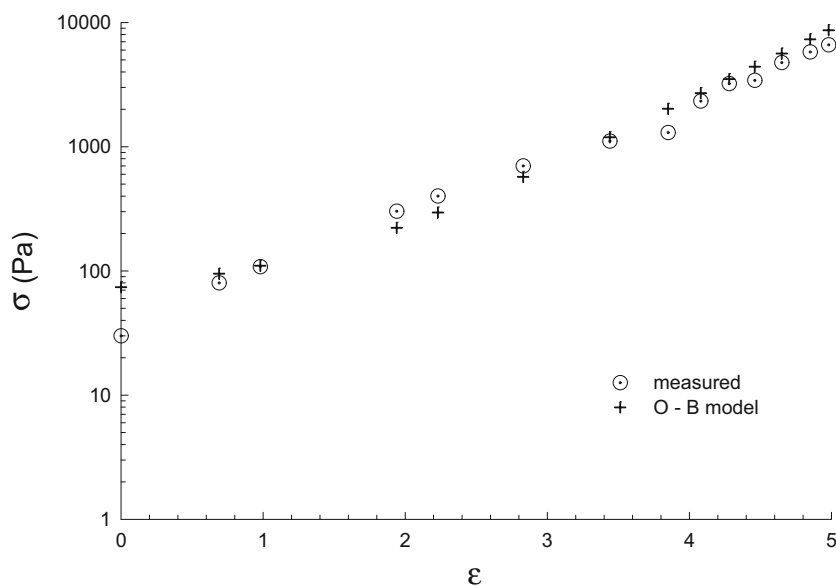
## Modelling the suspension rheology

The increase of relative viscosity ( $\eta_r$ ) with volume fraction in dilute suspensions with non-Newtonian matrices was predicted to follow the Einstein rule ( $\eta_r = 1 + 2.5\varphi$ ) by Koch and Subramanian (2008). The results in Table 1 show increases of 25, 66 and 182% for  $\varphi = 5, 10$  and 20% respectively. The Einstein formula predicts 12.5, 25 and 50% increases. It is surprising that the 5% results differ from the Einstein result by such a large amount. Generally the experimental values in Table 1 for the increases in relative viscosity are about twice the predicted values. We note that Vázquez-Quesada et al. (2019) have suggested a more refined computational method which gives results close to experiment for the 5% case.

The first normal stress difference was also predicted to increase by the same amount as the viscosity, but from Table 1, one sees that experiments show that increases of 27%, 133% and 260% occur for 5, 10 and 20% respectively, again much higher than the Einstein prediction.

The presence of a non-zero  $N_2$  shows that the Oldroyd-B model is not adequate to describe suspension rheology. (A simple solution for this problem is to replace the  $2\eta_s \mathbf{d}$  term

**Fig. 4** Axial stress as a function of Hencky strain for the steel ball case (circles)—the crosses are the Oldroyd-B model results. Rate of extension  $17.5 \text{ s}^{-1}$  corresponds to a Weissenberg number  $\dot{\epsilon}$  of 1.52. There is no steady state stress since  $Wi > 0.5$



in Eq. 1 by a Reiner-Rivlin term of the form  $2\eta_s \mathbf{d} + 4\nu_2 \mathbf{d}^2$ , where  $\nu_2 = N_2 \dot{\gamma}^2$ ; however, this inelastic contribution should not be expected to describe unsteady flows.)

Turning to the  $G'$ ,  $G''$  results, one might assume following See et al. (2016) that the relaxation time for the suspensions is the same as that of the matrix fluid and that the ratio of  $\eta_s$  to  $\eta_0$  remains at 0.68, which has been used to describe the matrix. These assumptions lead to results that are not close to experimental values. For example, for a 10% suspension at  $\omega = 10 \text{ rad/s}$   $G'$  is predicted to be 5.7 Pa, whereas experiment shows about 15 Pa; corresponding values of  $G''$  are 12 Pa and 53 Pa.

For the suspension uniaxial elongation tests (Fig. 7), the assumption that the relaxation time is 0.087 s leads to Weissenberg numbers below 0.5, so the dimensionless stresses ( $\sigma^*$ ) =  $\sigma/3\eta_0 \dot{\epsilon}$  are calculated to be of order 1.3 when the Hencky strain is 3, whereas Fig. 7 shows values near 100.

Clearly the Oldroyd-B single-mode model with  $\lambda = 0.087 \text{ s}$  does not come near to describing the experimental data for the suspensions.

We now consider a two-mode Oldroyd-B model. At exit from the tube in Fig. 2 where  $\epsilon$  is small, the fluid needs to support the weight of the embedded sphere immediately, so the assumption that the polymeric stress is then zero, which was used to derive Eq. 6, may not be realistic.

Hence, we assume that the polymer stress contribution is not necessarily relaxed at the beginning of the filament (exit from the funnel in Fig. 2) and at that point the Hencky pre-strain is  $\epsilon_0$ , so that in Eq. 6 we replace  $\epsilon$  by  $\epsilon + \epsilon_0$ . We also assume that there are two relaxation times ( $\lambda_1$  and  $\lambda_2$ ) and a corresponding set of viscosities  $\eta_1$  and  $\eta_2$  so there are two equations for the partial stresses of the form given in Eq. 6.

In order to generate significant axial stress in elongation,  $Wi$  must be greater than 0.5 for at least one of the modes.

As an example, we consider the 10% volume fraction data from Fig. 7.

To get an estimate of the effective Weissenberg number for the suspensions, we note that when  $Wi > 0.5$ , one term dominates the response for larger strains, and

$$\sigma^* \sim (2\eta_p/3\eta_0) \{ \exp(2-1/Wi)(\epsilon + \epsilon_0) - 1 \} / (2Wi - 1) \quad (9)$$

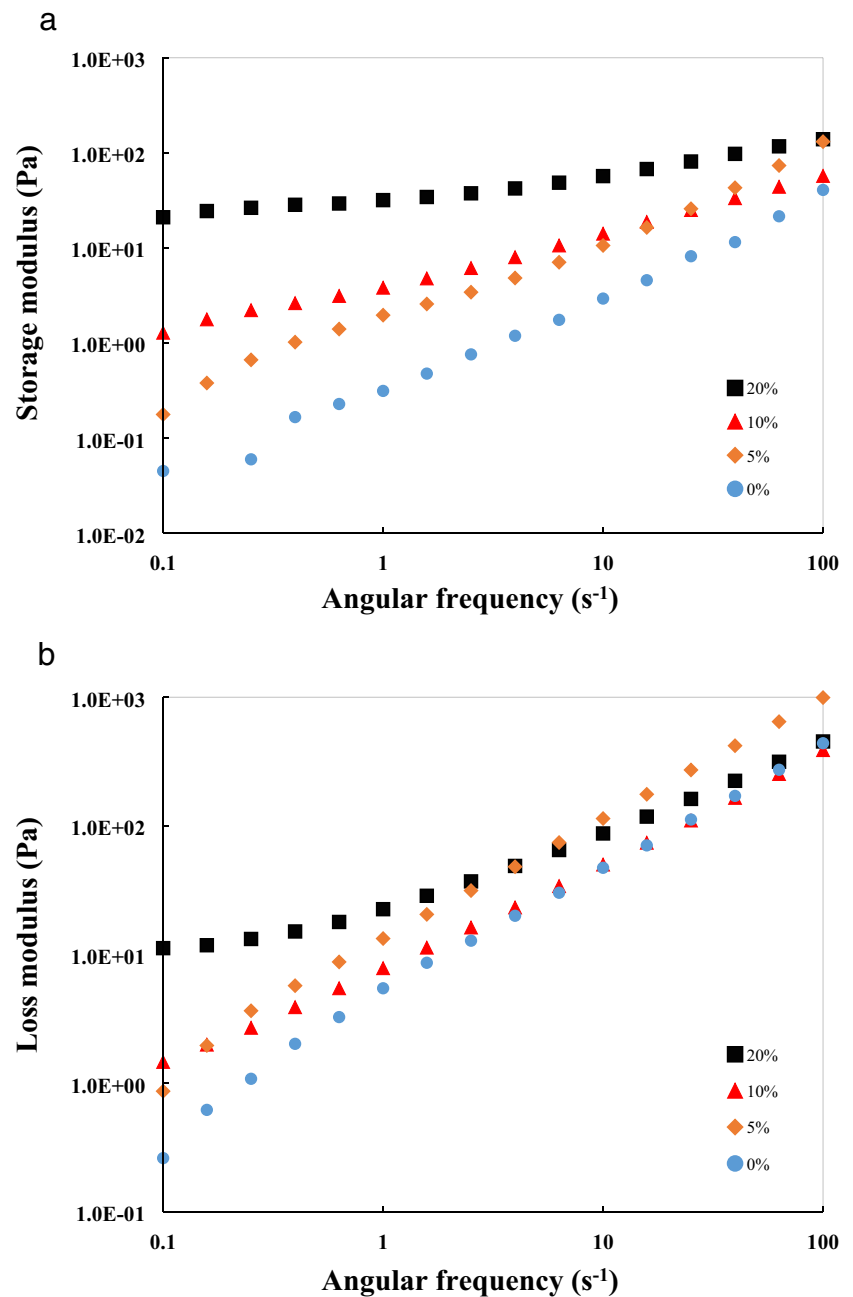
The strain has been augmented by a term  $\epsilon_0$  which is not yet determined. Equation 9 refers to the most active mode in the bimodal Oldroyd-B model. By differentiating Eq. 9 with respect to  $\epsilon$  one finds, approximately, and independent of  $\epsilon$  and  $\epsilon_0$ :

$$d\sigma^*/d\epsilon \sim (2-1/Wi) \sigma^*, \text{ or } d \ln \sigma^*/d\epsilon = 2-1/Wi \quad (10)$$

This predicts that the slopes of the lines in Fig. 7 should be constant in agreement with Eq. 10. The results found for  $Wi$  from Fig. 7 and Eq. 10 are shown in Table 3, together with the estimated properties of the two-mode Oldroyd-B model.

To find the parameters for the suspensions, we use the data of Fig. 7 and Eq. 10, finding that the effective Weissenberg number is 1.11 as shown in Table 3. Since the rate of elongation is  $2.56 \text{ s}^{-1}$  (Table 2), the dominant relaxation time ( $\lambda_2$ ) must be 0.42 s. The smaller relaxation time ( $\lambda_1$ ) can be found from the  $G'$  data (Fig. 5a). At  $\omega = 100 \text{ s}^{-1}$ , the measured value of  $G' \sim 56.4 \text{ Pa}$ , and for this frequency the contribution of  $\lambda_2$  is only  $\sim 1 \text{ Pa}$ . Hence, since  $\eta_1$  is about 1 Pa.s,  $\lambda_1$  needs to be around 0.01 s. If we set  $\lambda_1 = 0.01 \text{ s}$ , then to match  $G'(100)$ , the value of  $\eta_1 \sim 1.00 \text{ Pa.s}$ . To maintain  $N_1/\dot{\gamma}^2 = 0.271$  (Table 1),

**Fig. 5** Small-strain responses  $G'$  and  $G''$  for suspensions (1% strain). From bottom curves to top curves, 0, 5, 10 and 20% volume fractions respectively



one finds  $\eta_2 = 0.30$  Pa.s and to maintain the total shear viscosity at 3.58 Pa.s,  $\eta_s = 2.28$  Pa.s, so that  $\eta_s/\eta_0 = 0.64$ , close to the value for the matrix (0.68). Thus, the fit to the viscometric data is exact, but the fit of  $G'$ ,  $G''$  is not so accurate. If we now consider the elongational data from Fig. 7 for the 10% case, then one sees that if the initial strain is set to zero then the predicted  $\sigma^*$  is far too small—for example at  $\varepsilon = 3$ , with  $\varepsilon_0 = 0$ ,  $\sigma^* \sim 1.2$ , whereas Fig. 7 shows the measured  $\sigma^*$  to be  $\sim 76$ . Hence, a pre-strain of 3.8 units is needed to reconcile modelling and experiment.

The results in Fig. 7 are then well described, but the origin of  $\varepsilon_0$  is not clear; possibly the complex flow at exit from the

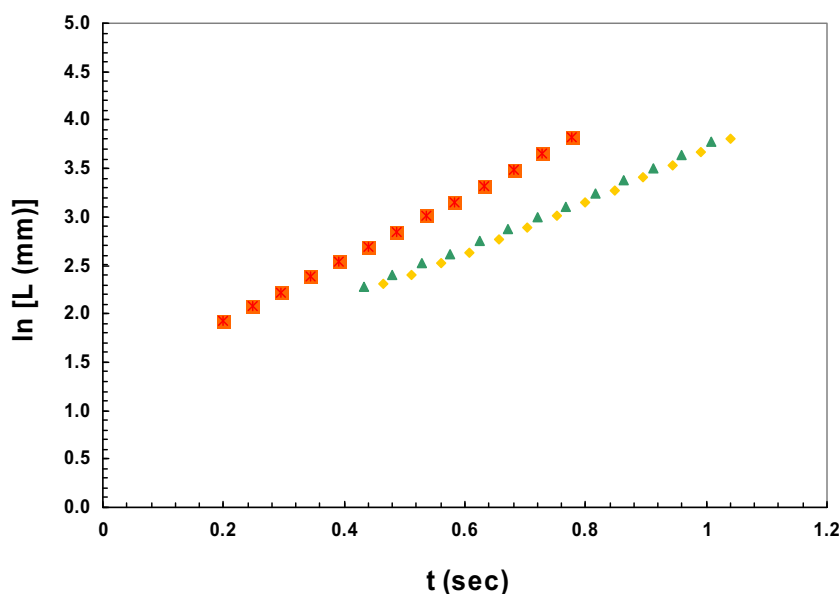
funnel (Fig. 2) is the cause because the fluid must resist the total load on the filament immediately upon exiting the nozzle.

Similarly, one can analyse the 5 and 20% volume fraction data and the results are shown in Table 3.

## Discussion

The matrix material used appears to be modelled quite well by a single-mode Oldroyd-B equation, but improvements in the correlation of the small-strain functions  $G'$ ,  $G''$  could be made

**Fig. 6** Length-time response of 5% (■), 10% (▲) and 20% (diamond). The time  $t$  is set so that at  $t=0$ , the length  $L=L_0$  is set to 3.2 mm, which is one ball diameter. All three curves extrapolate back to this value. The slope of the curves is constant and determines the elongation rates. These rates are 3.3, 2.56 and  $2.64 \text{ s}^{-1}$  for 5, 10 and 20% suspensions respectively



by using more relaxation times. The large discrepancy of orders of magnitude between experiment and an Oldroyd-B model in elongational behaviour of the matrix fluid found by Yang and Shaqfeh (2018) is not seen here—see Fig. 4.

If the procedure adopted for the suspensions is applied to the single-mode matrix fluid, then Fig. 7 and Eq. 10 show  $Wi = 1.02$ . Then it follows that  $\lambda = 0.058 \text{ s}$ ,  $\eta_p = 1.00 \text{ Pa}\cdot\text{s}$  and  $\eta_s = 1.16 \text{ Pa}\cdot\text{s}$  so that  $\eta_s/\eta_0 = 0.54$  instead of 0.68. Computing  $G'$  and  $G''$  for these values shows that the fit to the data is little better with the new values. From the elongational data in Fig. 7, one finds that a small initial strain of  $\epsilon_0$  of about 0.4 is sufficient to give agreement with experiment: it is also true that if one uses the original parameters ( $\lambda = 0.087 \text{ s}$ ) and allows an initial strain of  $\sim 0.4$ , then theory and experiment in Fig. 4 agree even better.

Clearly, the single-mode Oldroyd-B model is not adequate to describe the suspension responses. For the suspensions, the idea of using the same relaxation time as the matrix does not give a good description of  $G'$  and  $G''$  for these suspensions. Nor is this idea applicable to the uniaxial elongational data for the suspensions; the suspensions resist elongation much more than one expects when assuming a single-mode model with a low  $Wi$  of about 0.3.

**Table 2** Average extension rates ( $\dot{\epsilon}$ ) for various volume fractions ( $\varphi$ ) using embedded steel balls

$\varphi$ (%)	$\dot{\epsilon}$ ( $\text{s}^{-1}$ )
0	17.5
5	3.3
10	2.56
20	2.64

For the suspensions, the problem remains that for low  $Wi$ , there is no possibility of generating large stresses in extension with a single-mode model. This is confirmed by the calculations of Jain et al. (2019). Using various single-mode models, including an Oldroyd-B of the type used here, they found that the relative elongational viscosity of a dilute suspension is at most  $1 + 3\phi$  at a Hencky strain of 2.3, and decreases for larger strains. For a 5% suspension, this amounts to at most a 15% increase. A 15% increase is also predicted from the steady-state extensional analysis of Einarsson et al. (2018) for the 5% suspensions. In contrast, the experiments in Fig. 7 show a 10-fold increase.

If  $Wi \sim 2$ , one can see large deformations and hence stresses even in shear (Vázquez-Quesada et al. 2019). To achieve larger  $Wi$  values, either the effective elongation rate at the particle level has to be increased or the effective relaxation time has to be larger. Vázquez-Quesada et al. (2016) have shown that in denser suspensions (volume fraction = 0.4), shear rates much larger than the macroscopic shear rate can occur, but whether this is true for a suspension of volume fraction 0.05 in elongation is not known.

We now consider a two-mode Oldroyd-B model for the matrix fluid as a way of understanding the suspension behaviour from a microscopic (particle size) viewpoint. From Table 2, the average elongation rate is  $2.83 \text{ s}^{-1}$  and from Fig. 7, the average  $Wi$  for the three sets of suspensions is about 1.04. Hence, the most active relaxation time in elongation must be about 0.37 s. We shall assume that this is the value of the larger relaxation time  $\lambda_2$  for the matrix. A second shorter relaxation time  $\lambda_1$  of 0.09 s is assumed so that shear thickening occurs as before at  $Wi \sim 1$  in shear. Satisfying the requirements that the total viscosity  $\eta_0 = \eta_s + \eta_1 + \eta_2 = 2.16 \text{ Pa}\cdot\text{s}$  and that  $N_1/\dot{\gamma}^2 = 2\eta_1\lambda_1 + 2\eta_2\lambda_2 = 0.116$



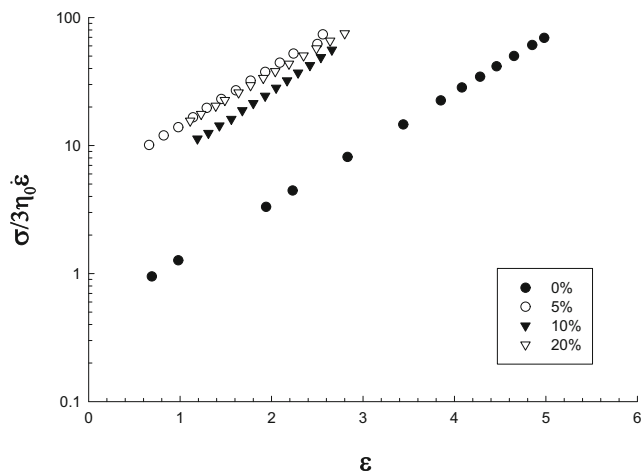


**Fig. 7** Dimensionless stress  $\sigma^*$  vs. Hencky strain  $\epsilon$  for matrix and suspensions

$\text{Pa}\cdot\text{s}^2$  still needs a further condition—here, we assume  $G'(100)\sim 4.6$  Pa (Fig. 1a). This gives the values ( $\eta_s$  is the Newtonian component of the viscosity)

$$\begin{aligned} \lambda_1 = 0.09\text{s}, \eta_1 = 0.414 \text{ Pa}\cdot\text{s} : \lambda_2 = 0.37\text{s}, \eta_2 \\ = 0.056\text{Pa}\cdot\text{s}; \eta_s = 1.690 \text{ Pa}\cdot\text{s}. \end{aligned} \tag{11}$$

The fit of  $G'$  and  $G''$  is improved from the single-mode model (Fig. 8a, b).

The elongational response is too low if Eq. 6 is used. By assuming that the elongational strain  $\epsilon$  is augmented from what is observed by an initial strain  $\epsilon_0$ , whose magnitude is around 4, agreement between experiment and the model can be found. With this matrix model, one can generate large stresses via the  $\lambda_2$  mode; one imagines at the microscopic level that pairs of spheres separate from one another with a small  $L_o$  at around the mean elongation rate ( $\dot{\epsilon}$ ).

We can estimate the shear-thickening properties of the 5% suspension using the two-mode Oldroyd-B model for the matrix by assuming that the formula of Einarsson et al. (2018), which was developed for a single-mode Oldroyd-B model, also holds for the two-mode model. Einarsson et al. (2018) found that the relative viscosity was expressed, to order  $\varphi Wi^2$ , as follows:

**Table 3** Effective Weissenberg numbers ( $Wi$ ), relaxation times ( $\lambda_1, \lambda_2$ ) and pre-strains for matrix and suspensions modelled by a two-mode Oldroyd-B model

$\varphi$ (%)	$Wi$	$\eta_1$ (Pa.s)	$\lambda_1$ (s)	$\eta_2$ (Pa.s)	$\lambda_2$ (s)	$\eta_s$ (Pa.s)	$\epsilon_0$
0	1.52	0.691	0.087	-	-	1.469	0
5	1.06	1.06	0.007	0.21	0.32	1.42	3.8
10	1.11	1.00	0.010	0.30	0.42	2.23	3.8
20	0.95	2.92	0.010	0.51	0.36	2.43	4.8

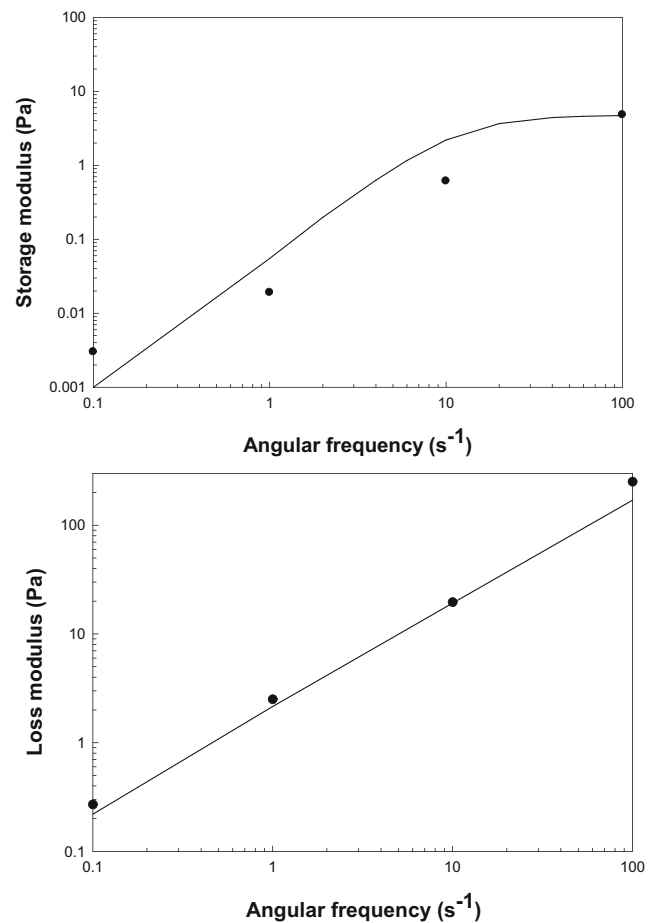


**Fig. 8**  $G', G''$  for two-mode matrix model (—) compared with experiment ( $\bullet$ )

$$\eta_r = 1 + 2.5\varphi + (0.62 - 0.03\beta) \varphi \beta Wi^2 \tag{12}$$

Here  $\beta = \eta_p/\eta_o$  for the single-mode model. For the two-mode model we assume, from Eq. 11, that  $\beta \sim 0.026$  so that the final term in Eq. 12, for the 5% suspension, is  $0.0008Wi^2$ . For a shear rate of  $10\text{s}^{-1}$ , where shear thickening is observed to begin (Dai et al. 2014),  $Wi = 3.7$  based on the long relaxation time (0.37 s). Hence, the final term in Eq. 12 is around 0.011 in this case, which is much smaller than the value seen experimentally. Similarly, the contribution to the relative viscosity from the shorter relaxation time (0.09 s) is also small, about 0.005 for a 5% suspension at  $Wi = 0.9$ . Hence, the analysis (12) does not seem to explain observed shear thickening.

Regarding the initial strains, one can see that the axial stress at  $t = 0$  must be non-zero due to the weight of the embedded ball which must be supported. It is thus probable that the complex flow at the inlet responds to the demands of the loaded, extending filament leading to the initial strain.

## Conclusion

In conclusion, it is clear that extreme caution must be taken when choosing a model for computation of viscoelastic suspension properties. From the microscopic point of view, a single-mode Oldroyd-B model is possibly adequate to describe the matrix rheology, but it is not useful to describe the macroscopic or microscopic behaviour of suspensions, and even a two-mode Oldroyd-B model gives only fair results for  $G'$  and  $G''$ . These factors need to be taken into account before engaging in massive computations if one is seeking to reconcile experiment and computation because the large local extensions seen by Hwang et al. (2004) depend on the elongational model, and in turn they augment the axial stress.

In addition, as the work of Vázquez-Quesada et al. (2019) has shown, the details of the computational procedures are also important and multiple-sphere cell computations lead to results quite different from those found in earlier investigations (for example Shaqfeh 2019; Tanner 2019; Vázquez-Quesada et al. 2016; Yang et al. 2016) where a single sphere to a cell was used. Hence, improvements in experiment, modelling and computational strategy are still needed.

## References

- Dai SC, Qi F, Tanner RI (2014) Viscometric functions of concentrated non-colloidal suspensions of spheres in a viscoelastic matrix. *J Rheol* 58:183–198
- Einarsson J, Yang M, Shaqfeh ESG (2018) Einstein viscosity with fluid elasticity. *Phys Rev Fluids* 3:013301
- Hwang WR, Hulslen MA, Meijer HEH (2004) Direct simulations of particle suspensions in a viscoelastic fluid in sliding bi-periodic frames. *J Non Newt Fluid Mech* 121:15–33
- Jain A, Einarsson J, Shaqfeh ESG (2019) Extensional rheology of a dilute particle-laden viscoelastic solution. *Phys Rev Fluids* 4:091301(R)
- Koch DL, Subramanian G (2008) The stress in a dilute suspension of spheres suspended in a second order fluid subject to a linear velocity field. *J Non Newt Fluid Mech* 138:87–97
- Mahmud A, Dai SC, Tanner RI (2018) A quest for a model of non-colloidal suspensions with Newtonian matrices. *Rheol Acta* 57:29–41
- Metzner AB (1985) Rheology of suspensions in polymeric liquids. *J Rheol* 29:739–775
- See H, Jiang P, Phan-Thien N (2016) Concentration dependence of the linear viscoelastic properties of particle suspensions. *Rheol Acta* 39:131–137 (2000)
- Shaqfeh ESG (2019) On the rheology of particle suspensions in viscoelastic fluids. *AIChE J* 65:e16575
- Tanner RI (2000) *Engineering Rheology*, 2nd edn. Oxford Univ. Press
- Tanner RI (2019) Review: rheology of non-colloidal suspensions with non-Newtonian matrices. *J Rheol* 63:705–717
- Tanner RI, Dai SC, Qi F, Housiadas K (2015) Viscometric functions of semi-dilute non-colloidal suspensions of spheres in a viscoelastic matrix. *J Non Newt Fluid Mech*. 201:130–134
- Vázquez-Quesada A, Tanner RI, Ellero M (2016) Shear-thinning of non-colloidal suspensions. *Phys Rev Lett* 117:108001
- Vázquez-Quesada A, Español P, Tanner RI, Ellero M (2019) Shear-thickening of a non-colloidal suspension with a viscoelastic matrix. *J Fluid Mech* 880:1070–1094
- Yang M, Shaqfeh ESG (2018) Mechanism of shear thickening in suspensions of rigid spheres in Boger fluids. Part II: suspensions at finite concentration. *J Rheol* 62:1379–1396
- Yang M, Krishnan S, Shaqfeh ESG (2016) Numerical simulations of the rheology of suspensions of rigid spheres at low volume fraction in a viscoelastic fluid under shear. *J Non Newt Fluid Mech*. 234:51–68
- Zarraga IE, Hill DA, Leighton DT (2001) Normal stress and free surface deformation in concentrated suspensions of noncolloidal spheres in a viscoelastic fluid. *J Rheol* 45:1065–1084

**Publisher's note** Springer Nature remains neutral with regard to jurisdictional claims in published maps and institutional affiliations.